Antarct. Meteorite Res., **15**, 152–164, 2002

The reaction of forsterite with hydrogen – its apparent and real temperature dependences

Daisuke Kuroda and Akihiko Hashimoto

Graduate School of Earth and Planetary Sciences, Hokkaido University, Sapporo 060-0810

Abstract: We have studied experimentally the reaction rate between solid forsterite and hydrogen gas, one of the most fundamental reactions in the solar nebula. It was found that the rate-controlling gas species was atomic hydrogen rather than molecular hydrogen, from the linear dependence of the reaction rate on P_H. The temperature dependence of the reaction rate was determined both under constant P_{H_2} and under constant P_H conditions. The former, "apparent" activation energy of the reaction was estimated to be 86.5±4.8 (2 σ) kcal/mol. The latter, "real" activation energy was estimated to be 32.6±4.8 (2 σ) kcal/mol. From this, a general formula that gives the true reaction rate of forsterite with hydrogen was obtained:
$\log_{10}(J_F/\mathrm{g\ cm^{-2}s^{-1}}) = -32.6\ (\pm 4.8) \times 10^3/2.303\ RT + \log_{10}(P_H/\mathrm{atm}) + 4.00\ (\pm 0.07)$.

1. Introduction

In an effort to determine the reaction rate of the most fundamental mineral-gas reaction in the solar nebula, Nagahara and Ozawa (1996) carried out experiments on the Mg_2SiO_4 (forsterite)–hydrogen gas reaction at a single temperature 1700°C with variable hydrogen pressures, and concluded that the reaction rate was linearly proportional to the gas pressure of molecular hydrogen. Tsuchiyama *et al.* (1998) carried out experiments on the same system at variable temperatures with a single hydrogen pressure, 1.4×10^{-5} bar, and obtained the activation energy of the reaction, 372 kJ/mol (88.9 kcal/mol).

Hashimoto (1998) devised a new experimental configuration that enabled accurate controls over temperature, pressure, the dissociation reaction between H_2 and H, and recondensation of a product vapor, and conducted experiments on the forsterite–hydrogen reaction at 1500°C with variable hydrogen pressures. He reached the conclusion that it was atomic hydrogen, rather than molecular hydrogen, that reacted with forsterite, from the result that the reaction rate was linearly proportional to the concentration of atomic hydrogen. In his experiment, however, sintered, porous forsterite (porosity=34.5±6.8%) was used while it was assumed that the only outer surface of the sintered forsterite mass was accessible to reaction. It was found later that the reactive gas (*viz.* hydrogen) pervaded the forsterite through the pores, and enhanced the reaction rate uniformly. This was equivalent to increasing the surface area of forsterite by some uniform factor, which was calculated for the exposed exterior of the sample.

In order to have better control over the surface area, the present study used polished, polycrystalline forsterite with much less porosity (7.7±2.6%) than the charge used previously. We conducted experiments on the forsterite–hydrogen system at 1400°C with

variable hydrogen pressures to confirm Hashimoto's result for a different temperature. We also carried out experiments at 1200, 1300, 1400, and 1500°C at ~2×10^{-4} bar P_{H2}, and determined the reaction rate per unit surface area and unit time, and the activation energy.

2. Experiments

2.1. Apparatus and principle

Figure 1 is a conceptual illustration of the experimental system, which was also used by Hashimoto (1998). Molecular hydrogen is continuously fed at a rate controlled by a mass flow regulator into the reaction cell (made of Mo), which is set inside a high-temperature vacuum furnace. Figure 2 shows the inside of the reaction cell. The upper 2/3 of its volume is filled with fine-grained granules and foil strips of metallic tungsten as a catalyst. Hydrogen flows from the top through numerous narrow channels between the granules and strips, and undergoes many collisions with the tungsten surfaces. By the time it flows into the sample chamber, dissociation equilibrium has been established: $1/2\,H_2 \Leftrightarrow H$; $P_H = K(T)\,P_{H2}^{1/2}$, where $K(T)$ is the equilibrium constant and P's are partial pressures.

The mixed (molecular and atomic) hydrogen reacts with the sample, and product vapor as well as unreacted hydrogen are exhausted into the vacuum chamber through a long tube. The chamber is kept at a high vacuum with a large capacity vacuum diffusion pump (3000 liter/s). The resistance the inside wall of the tube exerts on the gas flowing

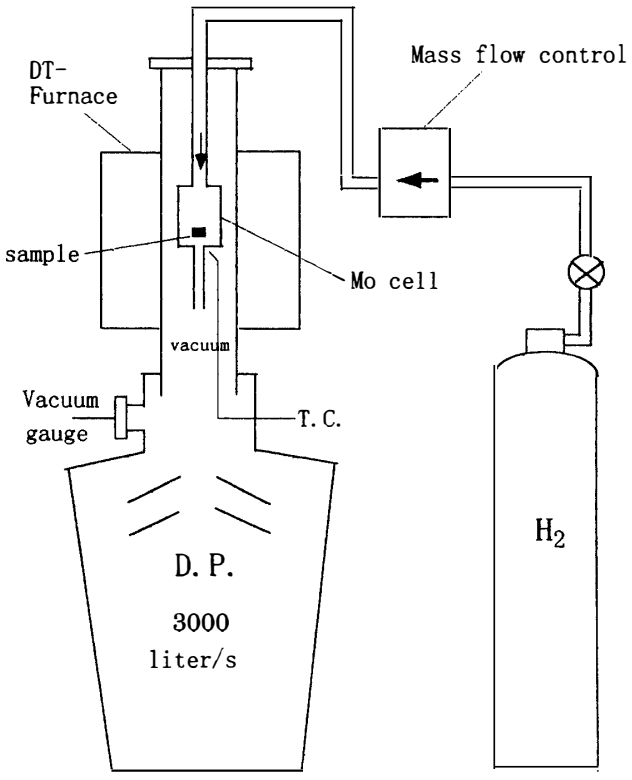

Fig. 1. Experimental system for the solid-hydrogen reaction. T.C.: thermocouple. D.P.: diffusion pump. DT-Furnace: Deltech DT-31-VT-68-C furnace.

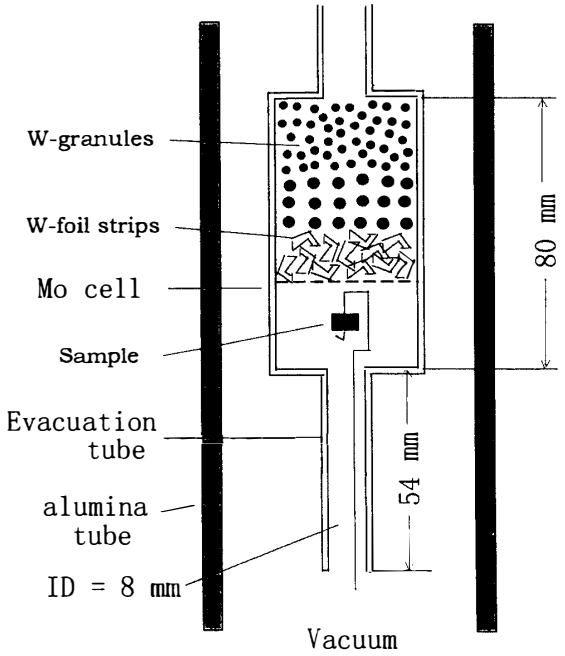

Fig. 2. Inside view of the reaction cell.

through it gives rise to a pressure increase in the sample chamber relative to the vacuum. When the pressure in the sample chamber P_1 at temperature T_1 is maintained by a flow rate f_0 of hydrogen through the flow meter at pressure P_0 and temperature T_0, conservation of mass leads to the following equation with U as the conductance of the evacuation tube in the molecular flow regime,

$$\frac{f_0 P_0}{RT_0} = \frac{U(P_1 - P_2)}{RT_1} = \frac{UP_1}{RT_1}, \quad U = \frac{d^3}{6L}\sqrt{\frac{2\pi RT_1}{M}}, \tag{1}$$

where R is the gas constant, P_2 the pressure at the tube outlet, M the mean molecular weight (~that of molecular hydrogen in the present experiment), and d (=0.80 cm) and L (=5.40 cm) the inner diameter and length of the tube, respectively. From the point of the tube outlet to the inlet of the diffusion pump the gas is evacuated through an alumina tube with a large inner diameter (d=55 mm, and L ~300 mm). The latter conductance is estimated to be ~20 times as large as U, thus P_2 ~1/20 P_1; P_2 is effectively negligible compared to P_1. P_0=1 atm and T_0=293 K. If f_0=20 cc/min and T_1=1773 K (1500°C), then P_1 ~P_{H2}=1.9×10^{-4} atm and P_H=3.9×10^{-6} atm from the dissociation equilibrium. The mean free path of hydrogen under these pressure and temperature conditions, ~2 cm, is larger than the diameter of the evacuation tube (0.8 cm), so the use of eq. (1) for U is justified (Hashimoto, 1999).

The product vapor is not immediately evacuated from the reaction cell for the reason described above. Naturally, some vapor molecules would change their direction and collide with the forsterite surface: a backward reaction would occur. Thus the value of J_{exp} measured in the experiment (as will be described below) is a 'net' reaction rate, which is the difference between the true reaction rate J_F and the backward reaction rate J_B. J_B should be proportional to the pressure of the product vapor around the sample, which in

turn is proportional to the sample surface area A and J_{exp}. Thus it is supposed that J_B is proportional to AJ_{exp}. If the tentative proportionality constant is expressed by χ, the equation becomes,

$$J_{exp} = J_F - J_B = J_F - \chi A J_{exp}. \quad (2)$$

In the experiment J_F is determined by the J_{exp} intercepts in AJ_{exp}–J_{exp} plots, using samples with several different surface areas.

2.2. Dissociation equilibrium

We have taken a special care about the dissociation of H_2 (because the reaction is endothermic), by using a catalyst (abundant tungsten metal) to guarantee dissociation equilibrium. The effectiveness in achieving equilibrium dissociation between H_2 and H in the present experiment can be evaluated from previous experimental investigations. Several works have indicated that tungsten is the best material for providing effective dissociation by surface catalysis. Moore and Unterwald (1964), in experiments using several different metallic materials, reported that ~40% of H_2 molecules incident on a tungsten surface at 2000 K dissociated into H atoms. In our experimental temperature range ~1500–1800 K, the dissociation efficiency per collision ranges from a few to 10% according to their result. Sutoh *et al.* (1995) studied the hydrogen cracking rate on a clean tungsten surface, and reported 1.5% efficiency per collision at 1873 K. At 1800 K we estimate that the dissociation degree of hydrogen at equilibrium is ~1%, as we noted in the previous section. Therefore, the reported cracking rate is high enough to obtain dissociation equilibrium given a few more collisions. The present experiment has used fine-grained (0.1–1.0 mm in approximate diameter), granular tungsten metal loaded in a 22 mm diameter × 30 mm height cylindrical volume, and strips (~1 × 3 mm) of tungsten foil loaded in 10 mm length beneath the granules. Under the circumstance each hydrogen molecule that flows into the molybdenum cell should experience at least 200 collisions with tungsten before entering the sample chamber. Thus dissociation equilibrium between H_2 and H is guaranteed. The H atoms created by dissociation are far more abundant than those consumed by the reactions between H and forsterite we describe in the following sections, because the sample surface is very small relative to the gas volume. Thus an equilibrium abundance of atomic hydrogen is maintained in the Mo cell under the experimental conditions described.

2.3. Samples and procedures

Forsterite samples were prepared from a 2:1 molar mixture of MgO and SiO_2 powder of 99.999% purity. They were pressed into pellets and reacted to forsterite in air at 1500°C for 12 hours. (In his previous experiments Hashimoto (1998) prepared his forsterite in the same way and machined them down to cylinders of different sizes. They had porosities of ~35%.) In the present experiments the reacted, porous forsterite was crushed to a fine powder, pressed into pellets, and sintered at 1400°C for 12 hours. They were machined into cylinders of six different sizes with small bore holes in the center, then sintered again in air at 1700°C for 20 hours to reduce porosity. Finally they were polished both on the top and bottom sides with a diamond paste (~1 μm in size). Except for the largest and smallest sizes, the cylinders were similar in shape, with the top and

bottom surface areas combined accounting for 65% of the total surface area. All samples remained slightly uneven (on a scale of 0.1 mm) on the circumferential surfaces due to a lack of polishing; the possible contribution of this unevenness to the effective surface area has not been taken into account.

The porosity of the samples was determined from the volume (assuming a perfect cylinder shape) and the specific gravity of forsterite (3.222). The average porosity for all the samples used was $7.7 \pm 2.6\%$. Its contribution to the effective surface area was also expected in the same level, *viz.* several %, because the pores were not interconnected but isolated. This contribution, however, has not been taken into account; only the macroscopic dimension measured by micrometer was used to determine the sample surface area. (The samples of Hashimoto (1998), on the other hand, are thought to have been permeable to gas down to some unknown depth due to partial connections between the pores; their effective surface area must have been much larger than but still proportional to the macroscopic estimation.)

A hydrogen flow of 2 cc/min was applied while raising the cell temperature at 10°C/min. The flow rate was changed to either 6.7, 20, or 60 cc/min (f_0 in eq. (1)) as soon as the maximum temperature was reached; this flow rate and the maximum temperature were then maintained for a prescribed period. When the cell temperature started falling (by shutting off the power supply; typically ~50°C/min for the first three minutes), the flow was switched to 2 cc/min again. The difference in sample weight before and after the experiment, the duration of heating at the maximum temperature, and the sample surface area averaged for before and after the experiment were combined to give J_{exp}, the net reaction rate of forsterite per unit time and unit surface area at the temperature and hydrogen pressure employed. The experimental duration was chosen so as to minimize the weight change; typically 2–5% of the initial weight was lost by reaction. The weight change during the temperature ramps (rising and falling) was minimal and is ignored.

3. Results and discussion

3.1. Pressure dependence

Table 1 and Fig. 3 show the present experimental results for the three different hydrogen pressures at 1400°C. A linear correlation was obtained for each pressure, as expected from eq. (2). According to this equation the backward reaction rate reduces to zero at infinitesimal A; in this limit the net reaction rate J_{exp} should be equal to the true reaction rate J_F. Thus J_F for each pressure was obtained from the y-intercept of the linear regression curve for that pressure. Figure 4 shows the correlation of the reaction rate J_F with the two pressure scales, P_{H2} and P_H. Here dissociation equilibrium was assumed between H_2 and H, from discussion in the previous section. A linear correlation was obtained for both pressure scales. The reaction rate is proportional to P_H (slope 1.05 ± 0.09), and to the square root of P_{H2} (slope 0.52 ± 0.05).

Figure 5 is the correlation of the reaction rate J_F with the two pressure scales, P_{H2} and P_H, determined at 1500°C by Hashimoto (1998) for a similar pressure range to ours. In his study the reaction rate was proportional to P_H (slope 1.01 ± 0.03), and to the square root of P_{H2} (slope 0.50 ± 0.02), consistent with our results. The absolute reaction rate (the Y-axis of the figure) in Hashimoto (1998) was overestimated by a factor of ~3, but

Table 1. Summary of experimental results.

T (°C)	P_{H2} (atm)	P_H (atm)	Δt (min)	A_1 (cm^2)	A_2 (cm^2)	W_1 (g)	W_2 (g)	S_1 (%)	S_2 (%)	J_{exp} (g/cm^2s)
1500	1.90E-04	3.90E-06	30	1.051	1.042	0.21428	0.21091	7.3	7.5	1.79E-06
1500	1.90E-04	3.90E-06	30	0.729	0.724	0.09214	0.08959	7.6	8.9	1.95E-06
1500	1.90E-04	3.90E-06	30	0.457	0.453	0.04563	0.04373	6.8	9.0	2.32E-06
1500	1.90E-04	3.90E-06	15	0.244	0.240	0.01848	0.01788	7.2	7.8	2.75E-06
1500	1.90E-04	3.90E-06	15	0.123	0.121	0.00593	0.00560	9.6	11.8	3.01E-06
1500	1.90E-04	3.90E-06	15	0.065	0.063	0.00263	0.00245	7.5	9.1	3.21E-06
1400	1.82E-04	1.54E-06	120	1.091	1.083	0.21552	0.21113	5.4	6.4	5.61E-07
1400	1.82E-04	1.54E-06	120	0.729	0.719	0.09405	0.09074	6.8	7.6	6.35E-07
1400	1.82E-04	1.54E-06	120	0.441	0.437	0.04424	0.04182	6.1	9.5	7.65E-07
1400	1.82E-04	1.54E-06	60	0.254	0.252	0.01866	0.01797	6.5	8.3	7.58E-07
1400	1.82E-04	1.54E-06	30	0.123	0.122	0.00614	0.00595	6.0	8.1	8.65E-07
1400	1.82E-04	1.54E-06	45	0.070	0.070	0.00295	0.00278	4.5	8.7	9.01E-07
1300	1.77E-04	5.42E-07	360	1.083	1.079	0.21233	0.21012	5.8	6.2	9.46E-08
1300	1.77E-04	5.42E-07	360	0.724	0.723	0.09308	0.09136	5.8	6.8	1.10E-07
1300	1.77E-04	5.42E-07	300	0.446	0.442	0.04521	0.04429	4.8	5.4	1.15E-07
1300	1.77E-04	5.42E-07	210	0.254	0.252	0.01918	0.01879	6.0	7.3	1.22E-07
1300	1.77E-04	5.42E-07	180	0.127	0.126	0.00637	0.00617	6.3	8.5	1.47E-07
1300	1.77E-04	5.42E-07	180	0.063	0.062	0.00247	0.00237	5.3	8.5	1.48E-07
1200	1.71E-04	1.66E-07	2400	1.030	1.024	0.20576	0.20277	7.9	8.3	2.02E-08
1200	1.71E-04	1.66E-07	2400	0.716	0.712	0.08897	0.08713	6.8	7.6	1.79E-08
1200	1.71E-04	1.66E-07	2160	0.448	0.443	0.04323	0.04207	7.8	8.5	2.01E-08
1200	1.71E-04	1.66E-07	2100	0.238	0.234	0.01755	0.01681	6.7	8.3	2.49E-08
1200	1.71E-04	1.66E-07	1200	0.131	0.130	0.00643	0.00630	6.9	7.5	1.38E-08
1200	1.71E-04	1.66E-07	1620	0.055	0.054	0.00176	0.00168	8.2	10.1	1.60E-08
1400	5.47E-04	2.67E-06	70	1.077	1.070	0.20759	0.20247	6.6	7.9	1.14E-06
1400	5.47E-04	2.67E-06	70	0.711	0.702	0.08485	0.08122	8.8	11.0	1.22E-06
1400	5.47E-04	2.67E-06	50	0.430	0.427	0.0402	0.03851	6.0	8.5	1.31E-06
1400	5.47E-04	2.67E-06	30	0.240	0.238	0.01572	0.01509	6.7	8.4	1.47E-06
1400	5.47E-04	2.67E-06	30	0.095	0.094	0.00248	0.00222	8.3	13.2	1.53E-06
1400	5.47E-04	2.67E-06	30	0.066	0.065	0.00254	0.00236	8.4	12.0	1.53E-06
1400	6.10E-05	8.93E-07	200	1.077	0.107	0.20834	0.20485	6.5	7.4	2.71E-07
1400	6.10E-05	8.93E-07	200	0.703	0.699	0.08514	0.08266	6.2	7.8	2.95E-07
1400	6.10E-05	8.93E-07	150	0.421	0.418	0.03771	0.03635	8.2	10.1	3.61E-07
1400	6.10E-05	8.93E-07	100	0.239	0.236	0.01576	0.01519	7.1	8.5	4.00E-07
1400	6.10E-05	8.93E-07	90	0.123	0.121	0.00648	0.00618	7.4	9.4	4.64E-07
1400	6.10E-05	8.93E-07	70	0.054	0.053	0.00167	0.00156	9.0	11.1	4.88E-07

T: temperature, P: pressure, t: heating duration, A: surface area, W: weight, S: porosity, J_{exp}: net reaction rate. Suffix 1 : denotes before the experiment, and suffix 2 : after the experiment.

uniformly, as is shown by experiments at the same temperature in the present study.

Both in Hashimoto (1998) and in the present experiment the total gas pressure (H_2 and H combined) is ~10^{-4} bar. At such a low pressure it is presumed that Langmuir adsorption equilibrium is established between gas and solid. In this case the

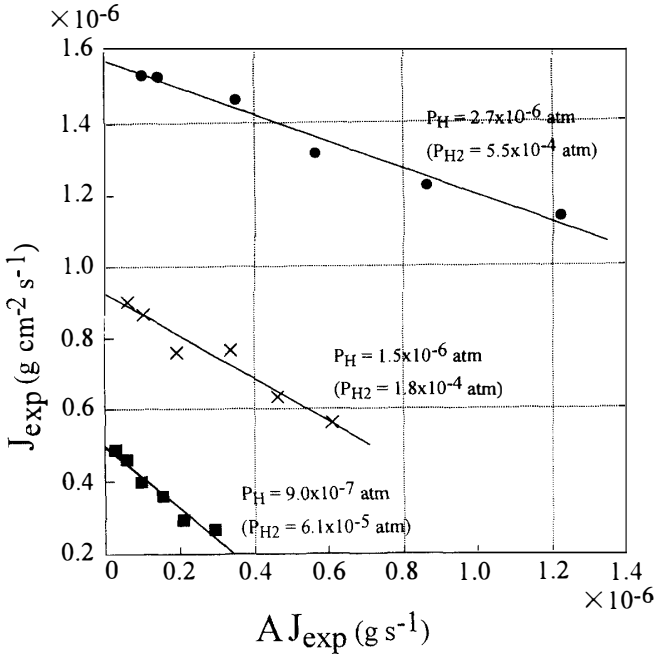

Fig. 3. Net reaction rates of forsterite with hydrogen at 1400°C for three different hydrogen pressures, obtained by three different H_2 flow rates 6.7, 20, and 60 cc/min at 293 K and 1 atm. Dissociation equilibrium is assumed between H_2 and H, from discussion in the text. Six data points for each pressure represent 6 experiments using different sample surface areas. The y-intercept of each linear regression curve gives the true reaction rate at 1400°C and the hydrogen pressure.

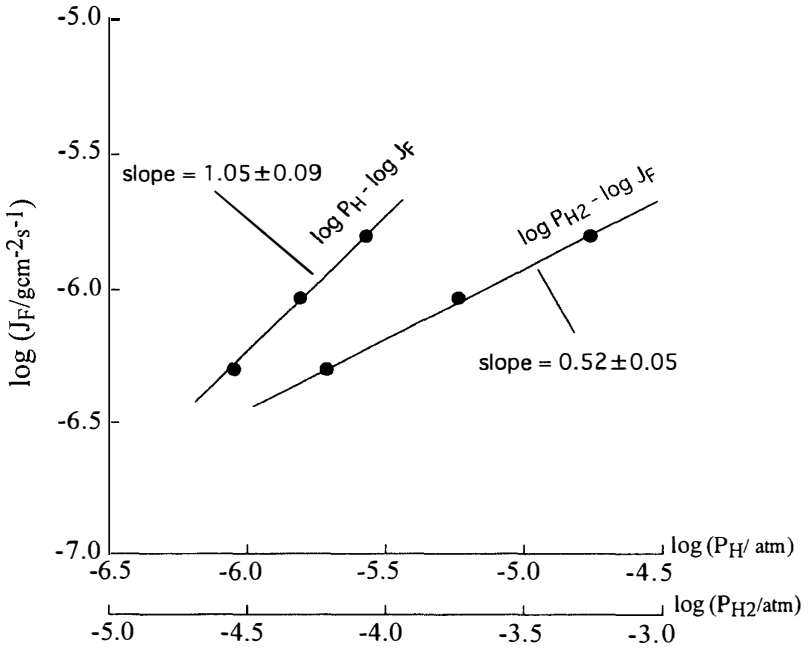

Fig. 4. The reaction rate of solid forsterite with hydrogen at 1400°C, shown as functions of P_{H2} and P_H. The present experiment. All scales are in log_{10} unit.

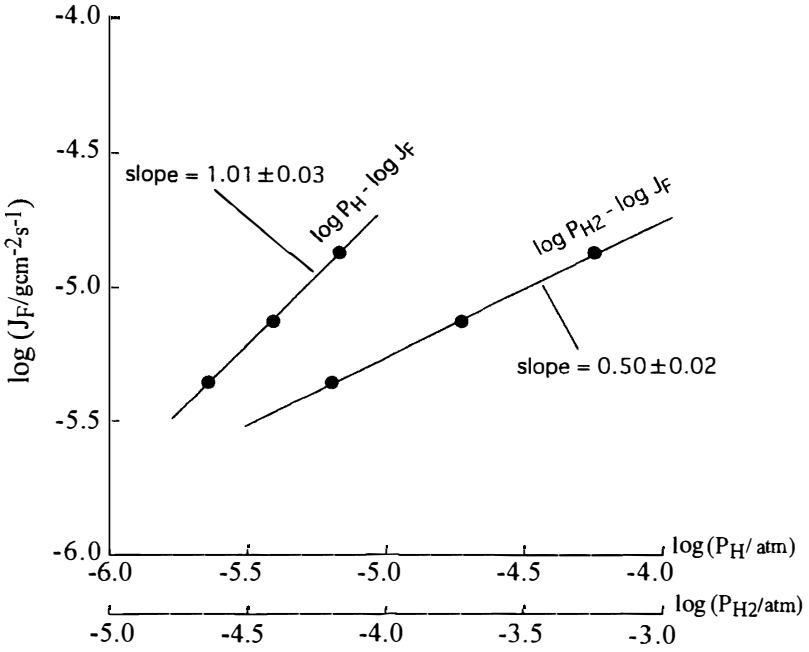

Fig. 5. The reaction rate of solid forsterite with hydrogen at 1500°C, shown as functions of P_{H2} and P_H after Hashimoto (1998). All scales are in log_{10} unit.

concentration of adsorbed gas on a solid surface is proportional to the partial pressure of the gas. Thus if adsorbed atomic hydrogen reacts directly with forsterite, the reaction rate should be proportional to the partial pressure of atomic hydrogen. The reason for the square root correlation to P_{H2} is simply explained by the dissociation equilibrium between H_2 and H.

3.2. Temperature dependence

Table 1 and Figs. 6a and 6b show the present experimental results for 1500, 1400, 1300 and 1200°C. A linear correlation was obtained for each temperature, as expected from eq. (2). For the same reason as in the pevious section J_F for each temperature was obtained from the y-intercept of the linear regression curve for that temperature. Figure 7 is an Arrhenius plot of the true reaction rate J_F *vs* temperature $1/T$. The data (open circles) and the linear regression curve labelled (a) denote original values of the y-intercepts from Figs. 6. These plots, however, may not be suitable for the present purpose because the hydrogen pressure in the reaction cell at each temperature is slightly different from one another due to the different thermal expansion while the same flow rate (20 cc/min at 293 K and 1 atm) was used for all the experiments. In order to compare data under the same pressure condition, the J_F values (open circles) were corrected for pressure differences using the linear relationship of the reaction rate with $P_{H2}^{1/2}$. The result is the points marked in crosses and their regression curve (b), where $P_{H2}=1.9\times10^{-4}$ atm (the actual P_{H2} at 1500°C) was chosen for reference. The slope of curve (b) gives the 'apparent' activation energy for the reaction between hydrogen and forsterite, 86.5± 4.8 (2σ) kcal/mol. Because P_{H2} is approximately equal to the total pressure in the nebula, curve (b) represents the reaction (*viz.* evaporation) rate of forsterite at a total pressure 1.9×10^{-4} atm, provided that dissociation equilibrium is established between H_2

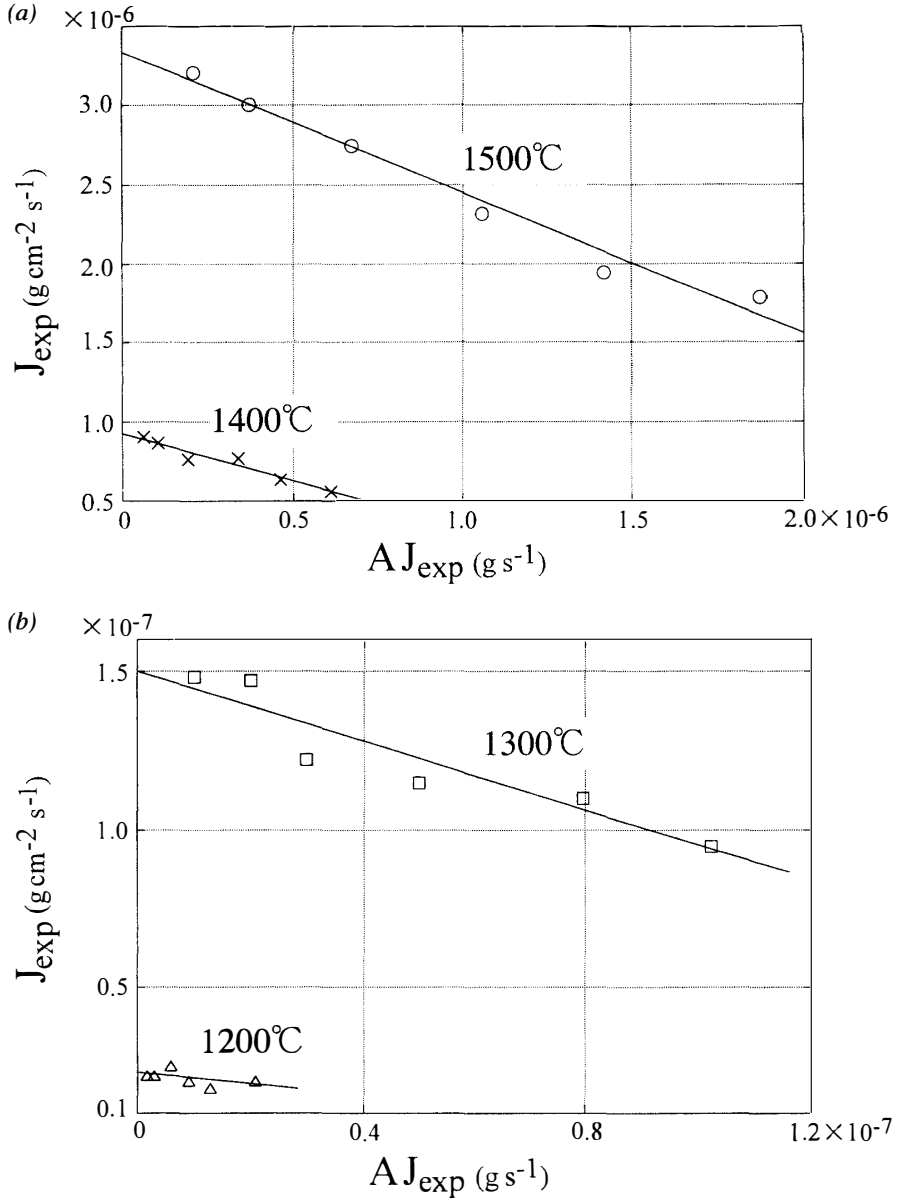

Fig. 6a, b. Net reaction rates of forsterite with hydrogen (flow rate fixed at 20 cc/min) at four temperatures. Six data points for each temperature represent 6 experiments using different sample surface areas. The y-intercept of each linear regression curve gives the true reaction rate at the temperature and the hydrogen flow rate.

and H.

Because the degree of dissociation is dependent upon temperature, the partial pressure of atomic hydrogen was not constant at the different experimental temperatures, even though the partial pressure of molecular hydrogen was kept nearly constant. Since Hashimoto (1998, 1999) and we have found that it was atomic hydrogen that actually reacted with forsterite, the 'real' temperature dependence of the reaction rate should be evaluated under a constant pressure of atomic hydrogen. Again, in order to compare data under the same pressure condition, the J_F values (open circles) were corrected for pressure

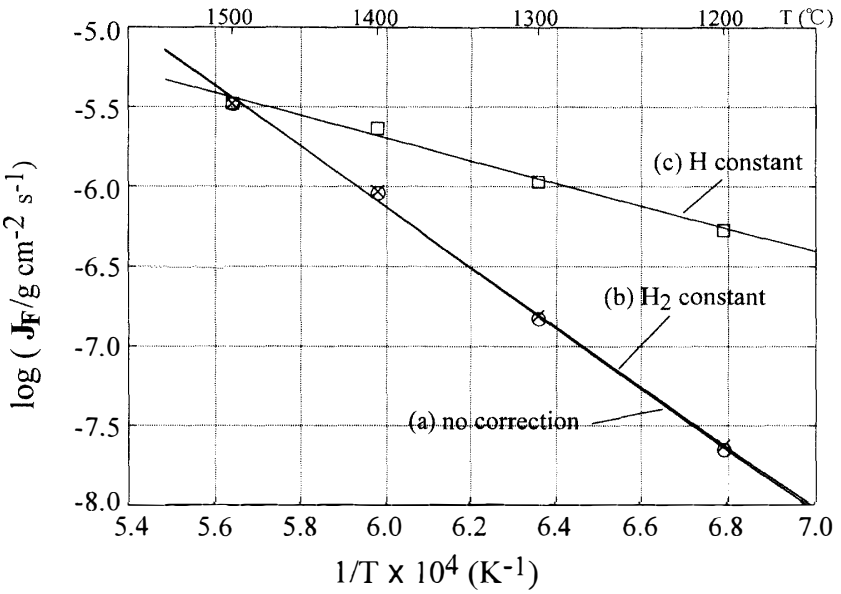

Fig. 7. Arrhenius plot of the reaction rate determined for the forsterite-hydrogen reaction. Open circles and their linear regression curve (a) denote the reaction rate J_F from the y-intercepts in Fig. 6. Crosses and curve (b) denote the J_F values corrected for P_{H2} to become constant (1.9×10^{-4} atm). Open squares and curve (c) denote the J_F values corrected for P_H to become constant (3.9×10^{-6} atm). Ordinate in $\log_{10}$ unit.

differences using the linear relationship of the reaction rate with P_H. The result is the points marked in open squares and curve (c), where $P_H = 3.9 \times 10^{-6}$ atm (the actual P_H at 1500°C) was chosen for reference. Then, the 'real' activation energy for the reaction between hydrogen and forsterite, determined from the slope of curve (c), is 32.6±4.8 (2 σ) kcal/mol. From this, a general formula that gives the true reaction rate of forsterite with hydrogen follows:

$$\log_{10}(J_F/\text{g cm}^{-2}\text{s}^{-1}) = -32.6\ (\pm 4.8) \times 10^3/2.303\ RT + \log_{10}(P_H/\text{atm}) + 4.00(\pm 0.07). \quad (3)$$

This formula is valid *whether dissociation equilibrium of hydrogen is achieved or not,* although the dissociation equilibrium was maintained in the experiment in order to control P_H.

The slope of the regression curves in Figs. 6a and 6b (χ value) appears to be dependent on temperature; it decreases as the temperature drops. We do not yet understand the cause of this effect, but obviously χ values contain information on the backward reaction, *viz.* condensation.

3.3. Comparison with the previous works

The present result is compared with earlier work in Fig. 8. The experimental configuration of Tsuchiyama *et al.* (1998) was different from ours. They used a long molybdenum crucible (16 mm ID and 124 mm in length) with its bottom end closed and its top end open to a chamber connected to a high vacuum system. A forsterite sample was suspended inside near the bottom. The lower 2/3 length of the crucible was subjected to radiation from a Ta heater. Hydrogen gas was fed into the chamber and its

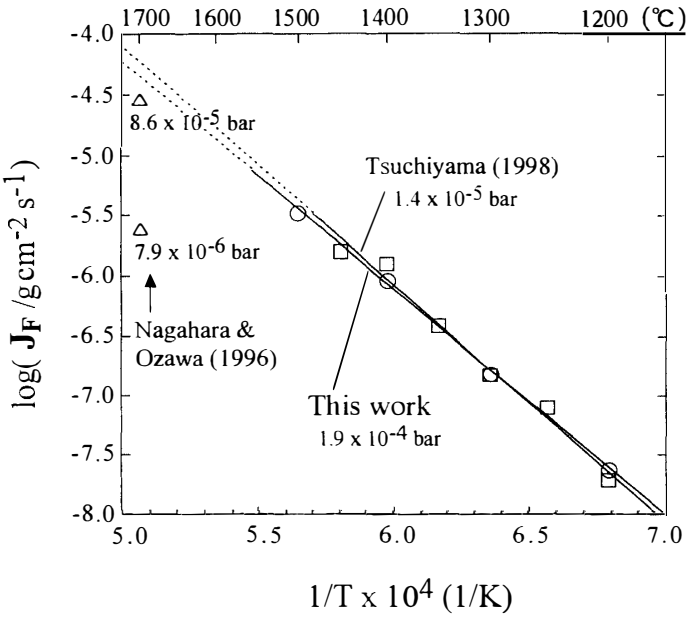

Fig. 8. Comparison of the present work and other experimental studies for the reaction rate of forsterite with hydrogen. Open circles (present experiment), open squares (Tsuchiyama et al., 1998) and open triangles (Nagahara and Ozawa, 1996). Values in bars indicate H_2 pressures. Ordinate in log_{10} unit.

pressure was monitored with a vacuum gauge mounted on the chamber. In this system, it is expected that the actual hydrogen gas pressure near the bottom of the crucible was different from that monitored with the gauge. We have made a calculation that assumed a steady state pressure gradient inside and along the molybdenum crucible. In the steady state the number of H_2 molecules that go into the mouth of the crucible is equal to that of H_2 molecules which go out of the mouth. To formulate the mass balance equation the temperature gradient along the crucible was also necessary; we assumed 1500 K for most of its length and also for the temperature of the gas which went out. The temperature of the gas that entered the mouth was assumed to be ~300 K (room temperature). From the geometry of the crucible, the temperatures, and the molecular flow regime appropriate to this system (Tsuchiyama *et al.*, 1998), we have estimated that the actual hydrogen gas pressure near the bottom of the crucible was ~14 times larger than that monitored with the gauge. Then the gas pressure 1.4×10^{-5} bar measured with the gauge is multiplied by 14 to give the actual hydrogen pressure around the sample, $\sim 2.0 \times 10^{-4}$ bar, which is close to the pressure of molecular hydrogen used in our system, $\sim 1.9 \times 10^{-4}$ bar. Thus Tsuchiyama *et al.*'s work is brought into agreement if a proper pressure correction is applied. The activation energy of the reaction obtained by them, 88.9 kcal/mol, is also in good agreement with the apparent activation energy, 86.5 ± 4.8 (2σ) kcal/mol, obtained by the present work.

On the other hand, the result of Nagahara and Ozawa (1996) is difficult to reconcile with our results. The pressure dependence of the reaction rate, which they claimed was proportional to P_{H2}, directly contradicts our result, that the reaction rate is proportional to P_H. It is possible that dissociative equilibrium between H_2 and H was not obtained in their case. Their experimental data, however, show significant scatter under constant

experimental conditions, making their determination of the pressure dependence less conclusive. Unlike the correction we made for Tsuchiyama *et al.* (1998), it is hard to reevaluate the H_2 pressure for Nagahara and Ozawa in the vicinity of the samples because it is not certain which flow regime the pressure belongs to, among the molecular, intermediate, and viscous flow regimes.

3.4. Implications

Using eq. (3), which is a general formula that gives the true reaction rate of forsterite with hydrogen, we can now discuss quantitatively the life time of a solid particle in the solar nebula. We assume that the nebular total pressure is approximately equal to P_{H2}, that the gaseous reactive species is atomic hydrogen only, and that dissociation equilibrium is maintained between H_2 and H. Figure 9 is an example: the time scale for complete evaporation of a solid forsterite spherule with an initial radius r_o, suspended in the nebula at temperatures and pressures. Here we note that the calculation considers only the forward reaction but ignores other effects including recondensation of a product vapor. The time scale for evaporation is also shown for vacuum evaporation of forsterite (Hashimoto, 1990). A solid particle of r_o=10 mm evaporates in 200 and 0.1 hours at 1500 K and 2000 K, respectively, in a hydrogen gas at $P_{H2}=10^{-3}$ bar, while in vacuum it takes 500000 and 5 hours, respectively. In this way the reaction with hydrogen (at 10^{-3} bar) reduces the evaporation time scale by 1/2500 at 1500 K and 1/50 at 2000 K compared to vacuum. This effect strongly constrains the origin and evolution of solid materials in the solar system.

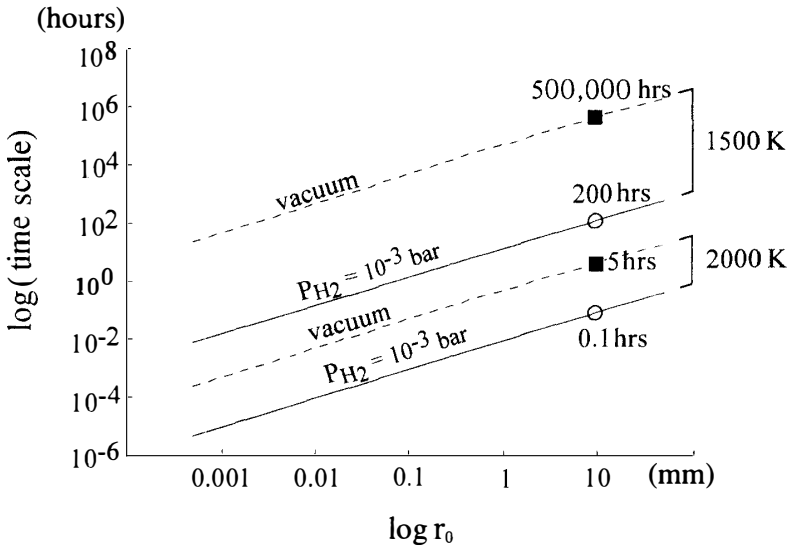

Fig. 9. Time scales for complete evaporation of a solid forsterite particle with an initial radius r_o, at several temperatures and pressures in the solar nebula. Solid lines denote the time scale for evaporation at $P_{H2}=10^{-3}$ bar, and broken lines that in vacuum (Hashimoto, 1990). Open circles and solid squares indicate the time scales for evaporation for r_o=10 mm.

4. Conclusion

The most fundamental mineral-gas reaction in the solar nebula, Mg_2SiO_4-hydrogen, is found to be rate-controlled by atomic hydrogen. Only the set of conditions P_H and temperature must be specified to quantitatively estimate the reaction rate of forsterite. The time scale for complete evaporation of solid mineral grains in the nebula with $P_{H2} > 10^{-5}$ bar is significantly shorter than that for vacuum evaporation, which imposes a strong constraint on the origin of solid meteoritic and planetary materials, *e.g.* Ca,Al-rich inclusions and chondrules in chondrites. However the effect of recondensation, which tends to counteract evaporation, is still unknown, and needs to be quantitatively assessed in future studies.

Acknowledgments

We thank Dr. H. Kojima for his patient editorial handling, and Dr. S. Tachibana, Dr. B. Fegley, Jr., and Dr. J. A. Wood for their constructive comments. This work was partly supported by the Ministry of Education grant #11640436 to A. H.

References

Hashimoto, A. (1990): Evaporation kinetics of forsterite and implications for the early solar nebula. Nature, **347**, 53–55.

Hashimoto, A. (1998): Absolute reaction rates of hydrogen with condensed phases in the nebula. Meteorit. Planet. Sci., **33**, A65.

Hashimoto, A. (1999): Chemical and isotopic fractionations in primordial nebula. Yuseijin, **8**, 266–282 (in Japanese).

Moore, G.E. and Unterwald, F.C. (1964): Thermal dissociation of hydrogen. J. Chem. Phys., **40**, 2639–2652.

Nagahara, H. and Ozawa, K. (1996): Evaporation of forsterite in H_2 gas. Geochim. Cosmochim. Acta, **60**, 1445–1459.

Sutoh, A., Okada, Y., Ohta, S. and Kawabe, M. (1995): Cracking efficiency of hydrogen with tungsten filament in molecular beam epitaxy. Jpn. J. Appl. Phys., **34**, L1379–L1382.

Tsuchiyama, A., Takahashi, T. and Tachibana, S. (1998): Evaporation rates of forsterite in the system Mg_2SiO_4–H_2. Mineral. J., **20**, 113–126.

(Received August 30, 2000; Revised manuscript accepted February 21, 2001)